Optics and Lasers in Engineering 46 (2008) 527–534

Contents lists available at ScienceDirect

Optics and Lasers in Engineering

journal homepage: www.elsevier.com/locate/optlaseng

Use of projection moiré for measuring the instantaneous out-of-plane deflections of composite plates subject to bird strike

W. Van Paepegem [a,*], A. Shulev [b], A. Moentjens [a], J. Harizanova [b], J. Degrieck [a], V. Sainov [b]

[a] Department of Mechanical Construction and Production, Ghent University, Sint-Pietersnieuwstraat 41, 9000 Gent, Belgium
[b] Central Laboratory of Optical Storage and Processing of Information (CLOSPI-BAS), Akad. G. Bonchev Street Bl. 101, Sofia 1113, Bulgaria

ARTICLE INFO

Article history:
Received 9 July 2007
Received in revised form
24 February 2008
Accepted 25 February 2008
Available online 14 April 2008

Keywords:
Projection moiré
Topography
Out-of-plane displacement
window Fourier
bird strike
Composite

ABSTRACT

For the new generation aircraft families, the use of fibre-reinforced plastics is considered for the leading edge of the wings. However, this leading edge is very prone to bird strike impact.

This paper presents the use of the projection moiré technique to measure the instantaneous out-of-plane deflections of composite plates subject to bird strike. Very strict constraints with regard to (i) high-speed image acquisition, (ii) vibrations of the impact chamber, and (iii) projection and observation angles, complicated substantially the development of the set-up. Moreover, the high frame rates (12,000 fps) required a very intensive illumination.

In the optimized configuration, a specially designed grating with gradually changing period is projected by means of special halide hydride lamps through one of the side windows of the impact chamber onto the composite plate riveted in a steel frame. The digital high-speed camera is mounted on the roof of the impact chamber and records through a mirror the object surface with the projected fringe pattern on it.

Numerical routines based on local Fourier transform were developed to process the digital images to extract the phase and the out-of-plane displacements. The phase evaluation is possible due to the carrier frequency nature of the projected moiré pattern. This carrier frequency allows separation of the unwanted additive and multiplicative fringe pattern components in the frequency domain via the application of a proper mask. The numerical calculations were calibrated for the bird strike on an aluminum plate, where the plastic deformation could be checked after the test.

1. Introduction

The application of fibre-reinforced plastics is increasing steadily in civil aircraft. The new generation aircraft families of Airbus and Boeing will have major structural components in composite (wing box, wings, rudders, tail planes, stiffeners, etc.). Also the use of fibre-reinforced plastics for the leading edge of the wings is considered. However, this leading edge is very prone to bird strike impact which is one of the major design criteria for this component.

Therefore the behaviour of composite components under bird strike impact should be studied extensively and adequate experimental set-ups should be used. Furthermore, it is important to gather as much information as possible during the impact event, so that comparison with dynamic finite element simulations is possible and developed damage models for the composite material can be validated.

This paper presents the use of the projection moiré technique to measure the instantaneous out-of-plane deflections of composite plates subject to bird strike. Very strict constraints with regard to (i) high-speed image acquisition, (ii) vibrations of the impact chamber, and (iii) projection and observation angles complicated the development of the set-up. Finally, numerical routines were developed to process the digital images, enhance the contrast and reconstruct the phase and out-of-plane displacement.

2. Materials and experimental set-up

The experimental set-up for bird strike impact was built in-house and has been developed for accelerating masses of maximum 1 kg up to speeds of 250 m/s.

The schematic of the bird strike set-up and its different components are shown in Fig. 1. The bird or a gelatine replica is placed inside a “sabot” (a plastic holder that must ensure the

* Corresponding author at:Department of Mechanical Construction and Production, Ghent University, Sint-Pietersnieuwstraat 41, 9000 Gent, Belgium.
Tel.: +32 9 264 42 07; Fax: +32 9 264 35 87.
E-mail address: Wim.VanPaepegem@UGent.be (W. Van Paepegem).

0143-8166/$ - see front matter © 2008 Elsevier Ltd. All rights reserved.
doi:10.1016/j.optlaseng.2008.02.010

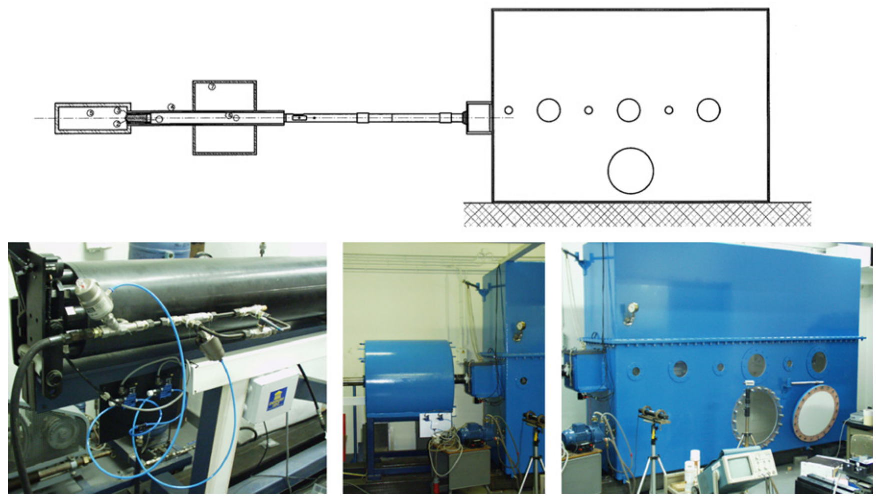

Fig. 1. Bird strike set-up with pneumatic accelerator, pressure relief chamber and impact chamber.

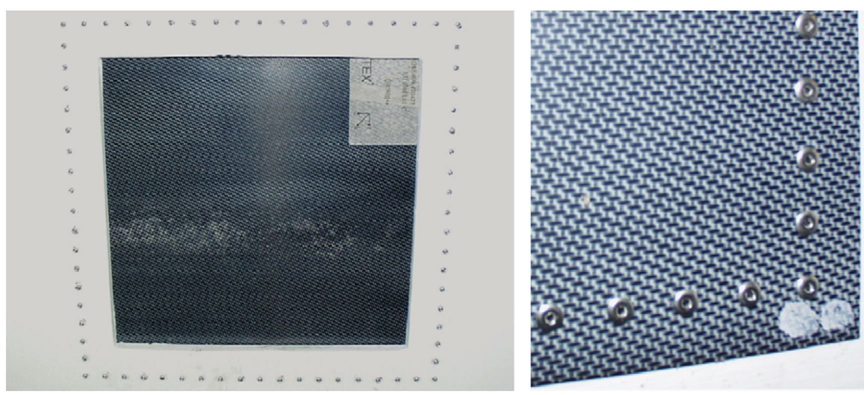

Fig. 2. View of the clamped carbon/PPS plate inside the impact chamber.

guiding of the bird) and is accelerated by a pneumatic gun (Fig. 1, bottom left). In the pressure relief chamber (Fig. 1, bottom middle), the pressure waves are relieved to reduce the vibrations and prevent early triggering of the lasers. Next, the sabot is stripped off and the (gelatine) bird enters the impact chamber (Fig. 1, bottom right). The impact chamber measures 4 m long-1 m wide $\times$ 3 m high.

Several observation windows in the side walls and the roof of the impact chamber allow for optical observation and triggering during the bird strike event. The speed of the (gelatine) bird at entrance of the impact chamber is measured by two lasers. The photodiodes trigger the digital high-speed camera to start recording.

The high-speed camera is a Photron Ultima APX-RS camera with 10 bit CMOS (Bayer system color, single sensor) with 17 μm pixels. The frame rate ranges from 60 to 250,000 fps. The maximum resolution is reduced accordingly.

The component under study was a carbon/PPS composite plate with dimensions of $400 \times 400\,\mathrm{mm}^2$ and a thickness of 2.50 mm. Fig. 2 shows the clamped carbon/PPS plate inside the impact chamber. The plate has been fixed with 74 rivets to make the comparison with riveted aerospace composite components as closely as possible.

A considerable part of the dynamic impact load is transferred from the impacted composite plate to the side walls of the impact chamber through the clamping frame on which the composite plate is riveted. This results in non-negligible vibrations of the impact chamber as a whole. As a consequence, all optical components that are fixed to the side walls or roof of the impact chamber will undergo large vibrations.

The main parameter of interest is the instantaneous out-of-plane displacement field during the bird strike impact. The maximum out-of-plane displacement of the composite plates is 20–30 mm under an impact of 800 g gelatine at a speed of 100 m/s.

For measuring such out-of-plane displacements, projection moiré seems the most suited optical technique. To prepare the experimental set-up, drawings of the interior of the impact chamber were made with the CAE software SolidWorks (see Fig. 3). This software allows then to measure all relevant distances in virtual space and as such, to choose the appropriate positions for the camera objective, the fringe projector, the mirrors and the light sources. This was relevant, because the location of the observation windows and the mounting frame imposed stringent restrictions on the projection and observation angles.

Based on the previous experience, it was considered that image acquisition at a frame rate of 12,000 fps would be acceptable. At this frame rate the resolution of the digital high-speed camera was maximum 512×512 pixels. One of the most difficult issues is to provide high-intensity fringe patterns, despite the limited sensitivity of the high-speed camera CMOS.

First holographic gratings were tested to generate the fringe pattern. Fig. 4 shows the projection device for the holographic grating that was constructed at the Bulgarian Academy of Sciences and the projected grating lines on a statically deformed plate

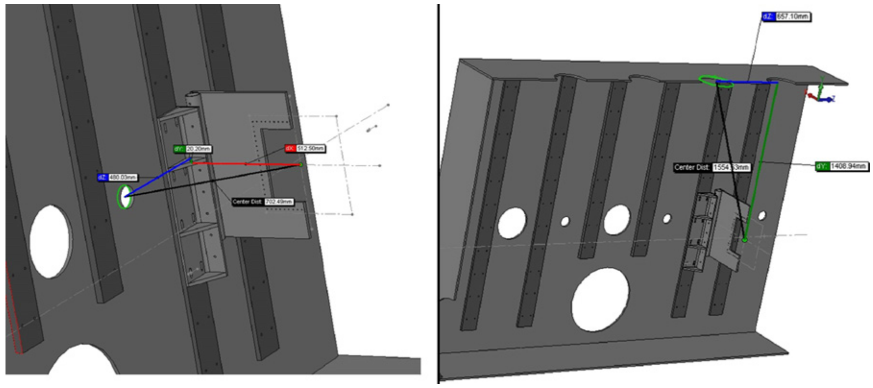

Fig. 3. SolidWorks drawings of the interior of the impact chamber.

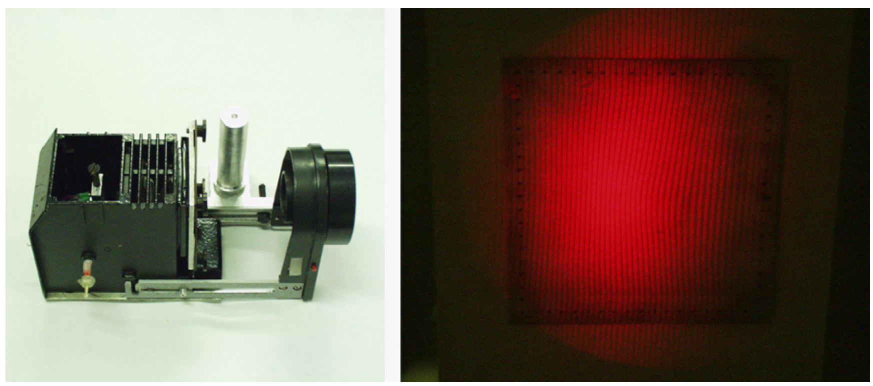

Fig. 4. Projection of grating lines with a holographic grating.

mounted in the impact test chamber. The diod laser was powered by batteries and had a limited power of 50 mW. When recording the same fringe pattern with the digital high-speed camera at a frame rate of 12,000 frames/s, no grating lines could be distinguished on the camera images. So a much stronger illumination was needed.

One option would be to use a much more powerful laser (of several Watt), but given the danger of working with such high-intensity lasers and the necessary water cooling, it was decided to switch to projection moiré with powerful white light illumination sources. The camera is equipped with special metal halide illumination sources (HEDLER MaxiBrite) that provide flicker-free light of constant intensity and a color temperature of approximately 6000 K.

In the next section, the applied projection moiré technique is discussed in detail.

3. Projection moiré technique

It is well known that projection moiré is a simple and reliable measurement technique [1–10] and in particular the Fourier transform profilometry [11–18] is extremely suitable for dynamic processes investigation.

Since the grating had to be projected from a small angle and a relatively short distance on the surface of the composite plate (due to the fixed location of the observation windows in the side walls of the impact chamber and their small sizes), diverging moiré fringe projection had to be used. In Fig. 5(a), the projection of the grating through the side window is displayed by the blue arrow, while the red arrow illustrates the way the deformed specimen is captured by the camera.

The theory that presents a diverging moiré fringe projection is well known and has been described in the literature [10]. The intensity distribution along the surface of the investigated object can be represented by the following equation:

$$I(x,y) = A(x,y) + B(x,y)\cos\left(2\pi\phi(x,y) + 2\pi\psi(x,y)\right) \tag{1}$$

where $A(x, y)$ is a slowly varying function representing the background illumination, $B(x, y)$ is a slowly varying function representing the contrast between light and dark fringes, $\phi(x, y)$ is the phase of the grating on the surface of the object and $\psi(x, y)$ is the phase of the object. From the geometry of the optical set-up shown in Fig. 5(b) the phase of the grating and the object can be described as

$$\begin{aligned} \phi(x,y) &= \frac{x}{P_0}\left(1 + x\frac{\sin\theta}{l}\right)^{-1}, \\ \psi(x,y) &= \frac{z(x,y)}{P_0\cos\theta}\left(\sin\theta + x\frac{(L - l\cos\theta)}{Ll}\right)\left(1 + x\frac{\sin\theta}{l}\right)^{-2} \end{aligned} \tag{2}$$

where $z(x, y)$ is the surface height of the object, θ is the angle between the optical axes of the projection and camera lenses, l is the distance from the projection lens to the origin of the coordinate system, L is the distance from the camera lens to the origin of the coordinate system, and P_0 is the period of the projected grating at $x = 0$. The previous equations are valid if the grating period P_0 is much smaller than the distance a between the lens and the projection grating ($P_0 \ll a$) and if the maximal surface height of the object z_{max} divided by the cosine of the angle θ is much smaller than the distance l ($z_{max}/\cos\theta \ll l$).

The phase of the projected grating on the surface of the object is not a linear function of x which means that the period of this grating varies along the width of the investigated object. This

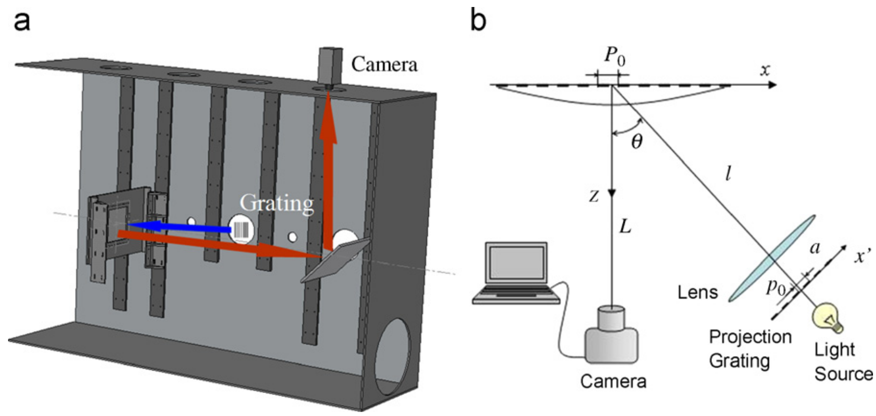

Fig. 5. (a) general scheme of the projection of the grating; (b) optical set-up for projection of grating lines onto the composite plate.

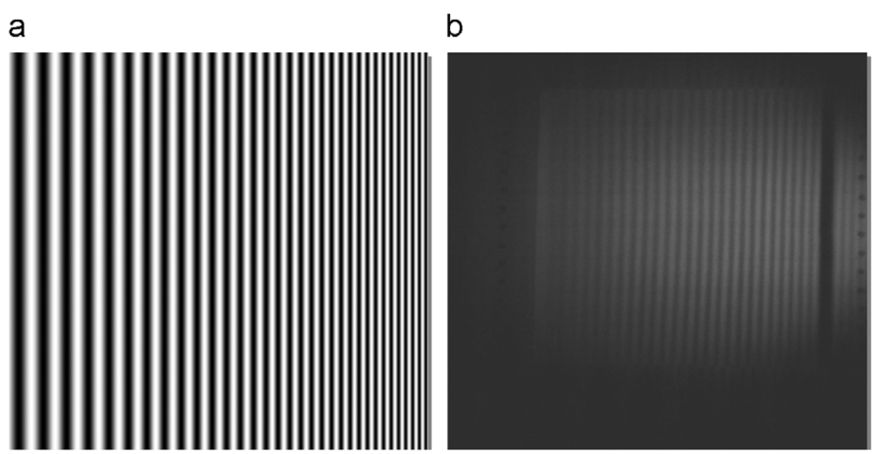

Fig. 6. (a) digitally synthesized projection grating; (b) projected grating on the surface of the composite plate before the bird strike.

nonlinearity does not allow applying the Fourier transform approach directly. To overcome this problem, a specially designed grating with gradually changing period could be used instead of a standard grating with constant period. In this manner a compensation of the changing fringe period could be achieved simply.

It can be easily derived that the phase of the projected fringe pattern remains linear along the object's surface if the phase of the projection grating is

$$\phi(x', y') = \frac{x'}{P_0}\left(1 - x'\frac{\tan\theta}{a}\right)^{-1} \tag{3}$$

where (x', y') is a coordinate system placed at the center of the projection grating, p_0 is the grating period at $x' = 0$, and a is the distance between the lens and the projection grating. In this way, taking into account the geometry of the experimental set-up, a digitally synthesized grating was printed on a slide and used as a projection grating. This grating is shown in Fig. 6(a) and the projected fringe pattern on the surface of the composite plate is shown in Fig. 6(b). It is clearly seen that the period of the projected pattern remains constant along the object's surface.

The phase of the projected fringe pattern and the phase of the object then can be written as

$$\phi(x, y) = \frac{x}{P_0}, \psi(x, y) = \frac{z(x, y)}{P_0 \cos\theta}\left(\sin\theta + x\frac{(L - l\cos\theta)}{Ll}\right). \tag{4}$$

Thus Eq. (1) can be represented in the usual way as

$$I(x, y) = A(x, y) + B(x, y)\cos(2\pi f_0 x + 2\pi\psi(x, y)) \tag{5}$$

where $f_0 = 1/P_0$ is the carrier frequency.

If the camera lens and the projection lens are placed at equal heights above the x–y plane then $L - l\cos\theta = 0$ and for the object phase we can get

$$\psi(x, y) = \frac{z(x, y)}{P_0}\tan\theta. \tag{6}$$

This formula is simple and commonly used in many applications to calculate the surface height where the optical set-up allows placing the camera and the lens at the same plane parallel to the object's surface. But in many real cases this is not possible and then the surface height of the object $z(x, y)$ must be calculated taking into account Eq. (4).

The camera is mounted on top of the impact chamber, but is not attached in any way to the chamber to avoid vibrations. The fringe projection is done through one of the side wall observation windows, but again without contact with the chamber. Due to the high power of the lamp (400 W), special heat resistant glass plates were used to mount the printed moiré grating in front of the illumination source.

Using this projection moiré technique, the projected fringes on an unloaded curved aluminum plate were recorded with the digital high-speed camera at a frame rate of 12,000 frames/s. Of course, all recorded images were the same, but this allowed to evaluate whether or not the light intensity was high enough and

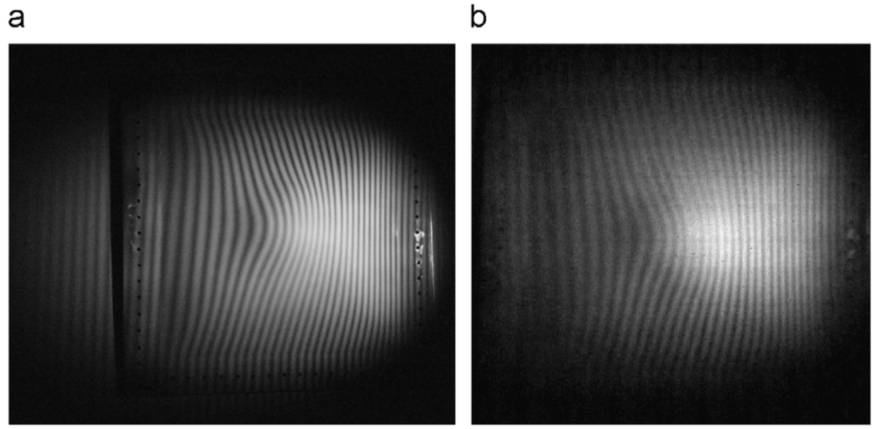

Fig. 7. Recording of the grating lines with (a) a standard digital camera, and (b) the high-speed camera at 12,000 fps.

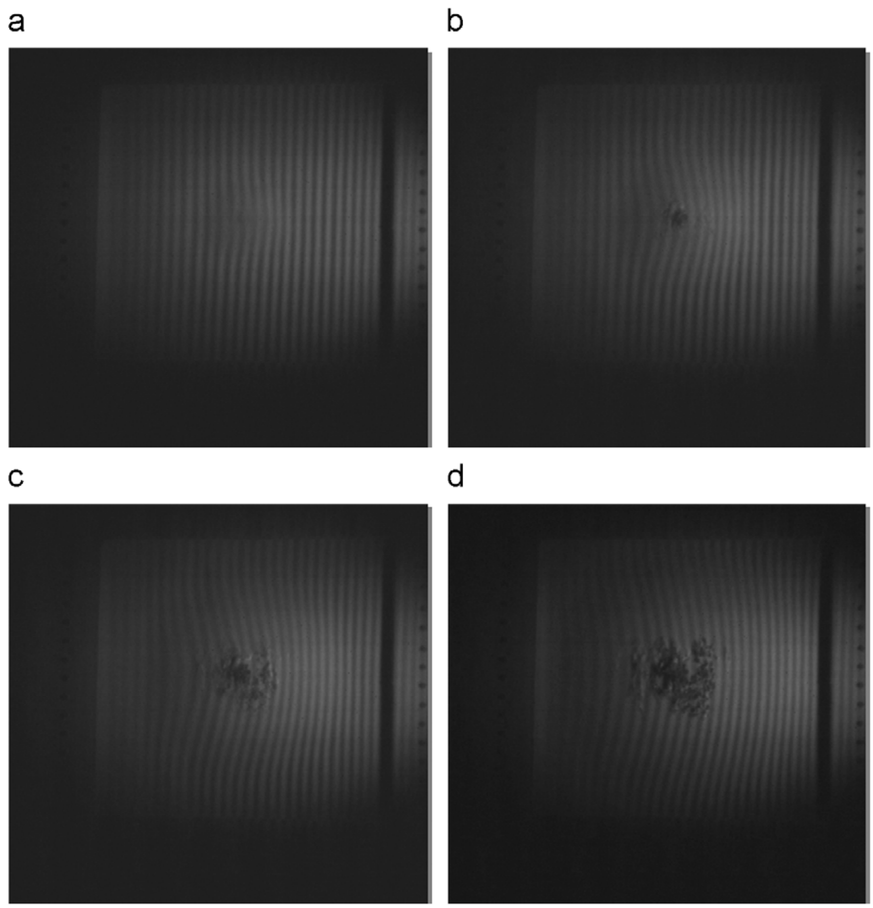

Fig. 8. (a–d) sequence of images of a bird strike impact on a riveted composite plate.

the blurring of the images was within acceptable limits. This appeared to be the case. Fig. 7(a) shows the recording of the projected grating lines with a standard digital camera and Fig. 7(b) shows the recording with the high-speed camera at 12,000 fps. There is enough illumination left to distinguish the grating lines.

Finally, a real bird strike test was recorded with the projection moiré set-up. Fig. 8(a–d) shows some of the recorded projection moiré images at 12,000 fps. In the lower images, the penetration of the bird through the composite plate can be clearly seen.

4. Numerical phase reconstruction

To extract the phase information from the recorded moiré fringe patterns, specialized software based on Fourier transformations was developed. The successive computational steps of the proposed algorithm are shown in Fig. 9. The phase evaluation is possible due to the carrier frequency nature of the moiré patterns. This carrier frequency allows separating the unwanted additive and multiplicative components of the fringe pattern in the frequency domain by applying a proper mask. Further trigonometric processing of the inverse Fourier permits exact phase map calculation.

To extract the phase information from the obtained moiré fringe patterns, specialized software based on the local Fourier transformations [19] or on the so-called Windowed Fourier Transform [20] was developed. The principle of this method relies on a movable window function which multiplies the investigated fringe pattern, resulting in many local subfringe patterns, and their Fourier spectra are calculated. This can be presented by

$$I_{AB}(u,v,a,b) = \Im\{I(x,y)W_{AB}(x-a,y-b)\} \tag{7}$$

where $\Im$ is the Fourier transformation, u and v are the spatial frequencies, $I(x, y)$ is the intensity distribution recorded by the camera and it can be represented theoretically by Eq. (5), $W_{AB}(x\text{-}a, y\text{-}b)$ is the window function, A and B correspond to the window dimensions, a and b are the shifting factors and $I_{AB}(u, v, a, b)$ is the local spectrum selected from this window function. The window function can be Gaussian, Hanning, Hamming, rectangular, and so on. In this paper we consider a rectangular window function:

$$W_{AB}(x-a,y-b) = \mathrm{rect}\left(\frac{x-a}{2A},\frac{y-b}{2B}\right) \tag{8}$$

where the dimensions of the window are $2A \times 2B$.

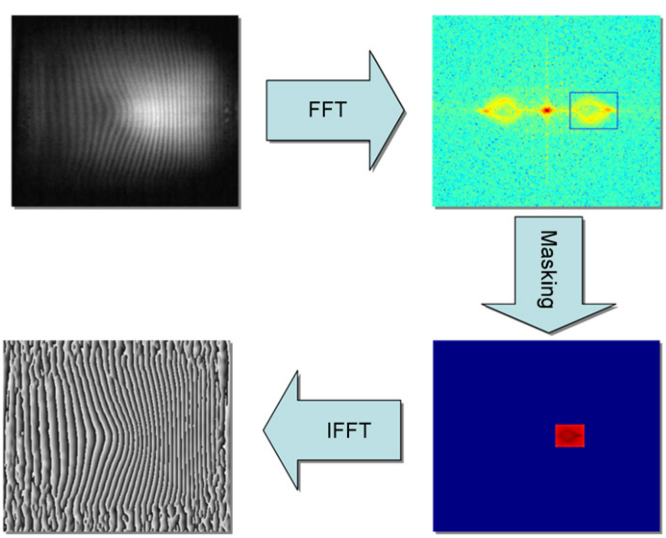

Fig. 9. Successive steps in the phase reconstruction of projection moiré fringes.

For each local Fourier spectrum half band frequency filtering [13], zero term and weak frequency suppression and inverse Fourier transformation are applied:

$$I_{AB}(x,y,a,b) = \Im^{-1}\left\{T_{\mathrm{thr}}\left\{\mathrm{I}_{AB}(u,v,a,b)\mathrm{rect}\right.\right.$$
$$\left.\left.\times\left(\frac{x-a}{A}-1,\frac{y-b}{2B}\right)\right\}\right\} \tag{9}$$

where T_{thr} is the thresholding operator which can be presented as

$$T_{\mathrm{thr}}\{x\} = \begin{cases} x & \text{if } x \geqslant \mathrm{thr} \\ 0 & \text{if } x < \mathrm{thr} \end{cases} \tag{10}$$

where thr is the threshold which can be estimated from the noise level in the fringe pattern individually for each local subfringe pattern [21,22]. This technique perfectly reduces the noise separately in each part of the fringe pattern. The phase distribution can be represented by

$$\Psi(x,y) = \iint \arctan\frac{\mathrm{Im}(I_{AB}(x,y,a,b))}{\mathrm{Re}(I_{AB}(x,y,a,b))}\,\mathrm{d}a\,\mathrm{d}b \tag{11}$$

where the integration is 2π modulated. The optimal window size depends on the specificity of the fringe pattern, mainly on the fringe density and noise level.

The presented phase extracting procedure is reliable for sophisticated fringe patterns and extremely robust against strong presence of noise which is typical for the high speed camera.

By means of the proposed algorithm, phase maps extracted from the captured fringe patterns during the bird strike impact are subtracted from the initial phase map corresponding to the object's surface before the impact.

The obtained phase maps can be unwrapped by means of different unwrapping algorithms [23]. At the end of the impact, part of the composite material is broken and therefore there are zones with lack of phase information. We have chosen the $Z\pi M$ algorithm [24] because it works well in the presence of singularity zones and can interpolate them naturally.

After the phase unwrapping and by means of Eq. (4) the deformation field has been calculated.

Fig. 10 first shows the reconstructed phase information for the recorded image (at 12,000 fps) of a curved aluminum plate in static position (see also Fig. 7(b)). This example was used to calibrate the developed software, because the predicted topology of the deformed aluminum plate could be easily compared with the experimentally measured out-of-plane profile. Also the accuracy of the proposed measurement technique has been verified with the aluminum plate. The maximal error is less than 1.5 mm and the mean error is approximately 0.5 mm.

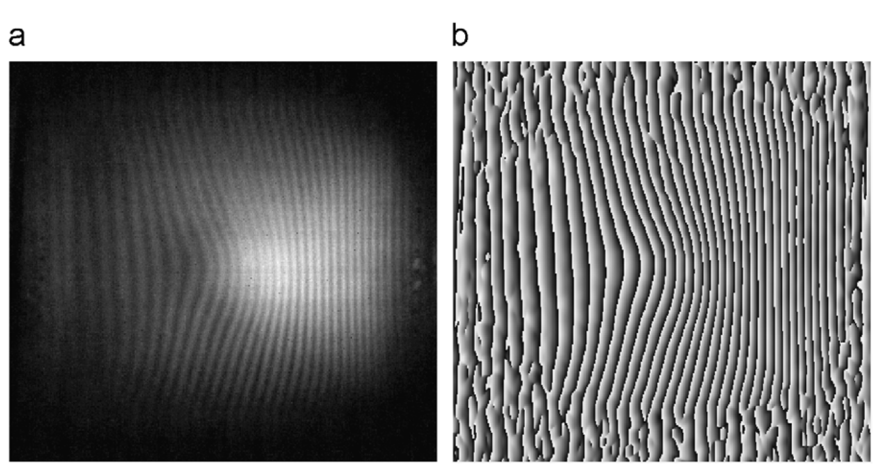

Fig. 10. (a) recorded projection moiré image (12,000 fps) of a curved aluminum plate in static position; (b) reconstruction of the phase map.

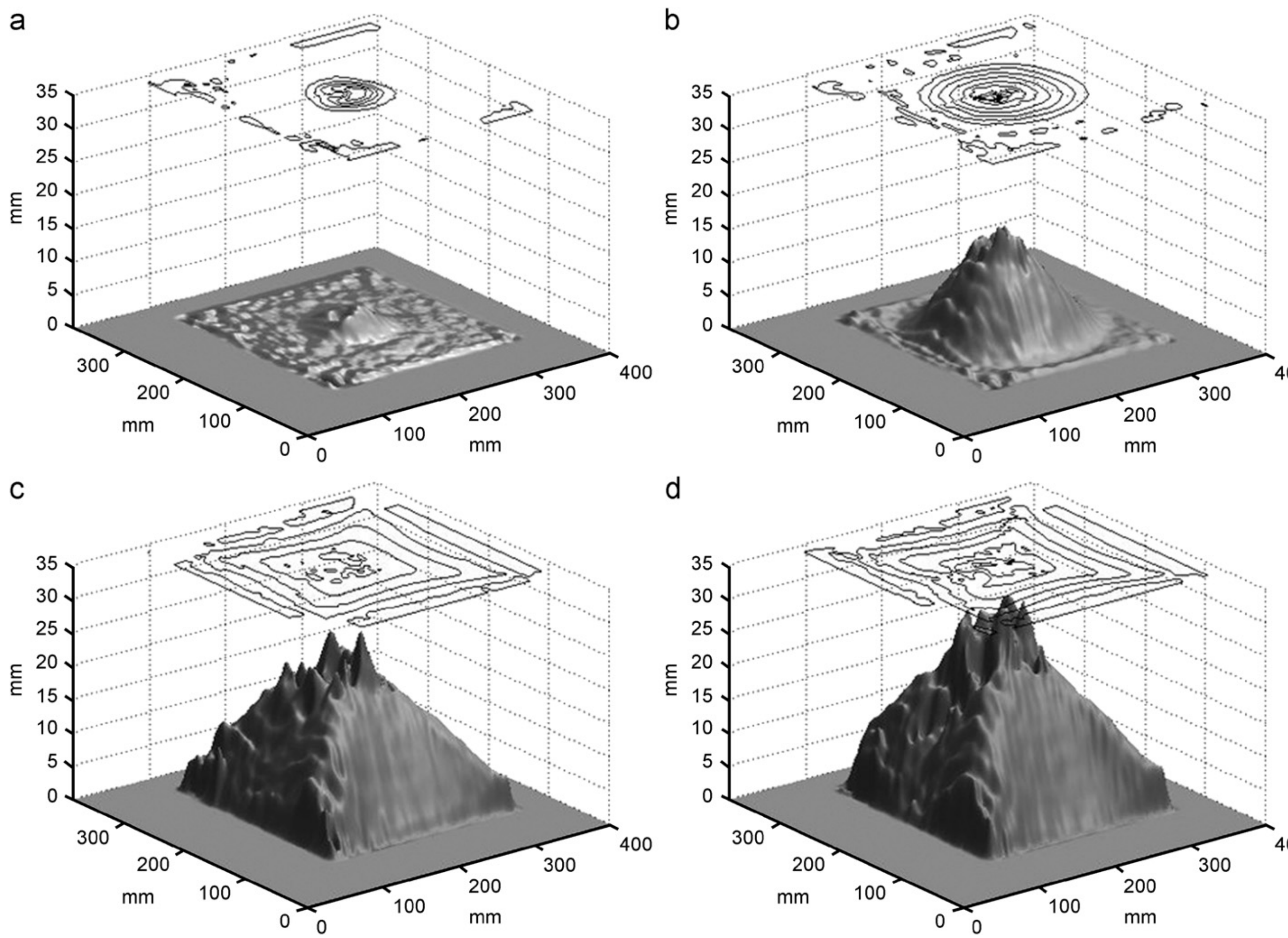

Fig. 11. (a–d) sequence of calculated out-of-plane displacement maps for the composite plate.

Finally Fig. 11 shows the out-of-plane displacement profiles for four successive frames during the bird strike event, which correspond with the recorded projection moiré images in Fig. 8. These data can now be used to compare the predictions of the finite element simulations with the experimentally measured instantaneous out-of-plane displacements during the bird strike event.

5. Conclusions

The feasibility of the projection moiré measurement has been investigated for real-time measurements of the out-of-plane displacement profile of a composite plate subject to bird strike. The main problem coming from the relatively short projection distance and big projection angle has been overcome introducing a digitally synthesized grating with gradually changing period. In this way compensation of the varying fringe period has been achieved.

To extract the phase information from the obtained moiré fringe patterns, specialized software based on the local Fourier transformations was developed. The phase evaluation is possible due to the carrier frequency nature of the moiré patterns. Usually the high-speed cameras offer low resolution and high noise levels which complicate most of the phase extracting algorithms. The natural filtering facilities of the proposed algorithm permit correct processing of the captured noisy data, reliability and exactness of the results. Further investigations are ongoing to increase the accuracy of the technique and to improve the automated processing of the successive digital frames.

Acknowledgments

The author W. Van Paepegem gratefully acknowledges financial support through a Grant of the Fund for Scientific Research—Flanders (F.W.O.). The authors are grateful to Ten Cate Advanced Composites for supplying the composite material, and to the Fund for Scientific Research—Flanders (F.W.O.) for the bilateral collaboration between UGent (Belgium) and CLOSPI-BAS (Bulgaria).

References

[1] Post D, Han B, Ifju P. High-sensitivity moire: experimental analysis for mechanics, materials. New York: Springer; 1994.
[2] Creath K, Wyant JC. Moiré and fringe projection techniques. In: Malacara D, editor. Optical shop testing. NewYork: Wiley; 1992.
[3] Rastogi PK, editor. Holographic interferometry principles and methods, Springer series in optical sciences, Vol. 68. Berlin: Springer; 1994.
[4] Kreis T. Handbook of holographic interferometry. Weinheim: Wiley-VCH GmbH; 2005.
[5] Idesawa M, Yatagai T, Soma T. Scanning moiré method and automatic measurement of 3-D shapes. Appl Opt 1977;16:2152–62.

[6] Yi-Bae C, Seung-Woo K. Phase-shifting grating projection moiré topography. Opt Eng 1998;37(3):1005–10.
[7] Peng X, Gao Z, Zhou SM. Surface contouring by a new type of digital moiré technique. Optik 1995;100(2):63–7.
[8] Peng X, Zhu Sm, Su Cj, Tseng Mm. Model-based digital moiré topography. Optik 1999;110(4):184–90.
[9] Purcell D, Davies A, Farahi F. Effective wavelength calibration for moiré fringe projection. Appl Opt 2006;45(34).
[10] Gasvik KJ. Optical metrology. NewYork: Wiley; 2002.
[11] Takeda M, Ina H, Kobayashi S. Fourier-transform method of fringe-pattern analysis for computer-based topography and interferometry. J Opt Soc Am 1982;72(1):156–60.
[12] Takeda M, Motoh K. Fourier-transform profilometry for the automatic measurement of 3-D object shapes. Appl Opt 1983;22(24):3977–82.
[13] Kreis T. Digital holographic interference-phase measurement using the Fourier-transform method. Opt Soc Am 1986;3(6):847–55.
[14] Su X, Chen W. Fourier-transform profilometry: a review. Opt Las Eng 2001;35:263–84.
[15] Su X, Chen W, Zhang Q, Chao Y. Dynamic 3-D shape measurement method based on FTP. Opt Las Eng 2001;36:49–64.
[16] Li J, Su X, Guo L. Improved Fourier-transform profilometry for the automatic measurement of three-dimensional object shapes. Opt Eng 1990;29(12):1439–44.
[17] Yi J, Huang S. Modified Fourier-transform profilometry for the measurement of 3D steep shapes. Opt Lasers Eng 1997;27(5):493–505.
[18] Mao X, Chen W, Su X. Improved Fourier-transform profilometry. Appl Opt 2007;46(5):664–8.
[19] Shulev AA, Roussev IR, Sainov V. New automatic FFT filtration method for phase maps and its application in speckle interferometry. Proc SPIE 2003;4933:323–7.
[20] Kemao Q. Windowed Fourier transform for fringe-pattern analysis. Appl Opt 2004;43(13):2695–702.
[21] Donoho D, Johnstone I. Ideal spatial adaptation via wavelet shrinkage. Biometrica 1994;81:425–55.
[22] Shulev A, Gotchev At, Foi Al, Roussev I. Threshold selection in transform-domain denoising of speckle pattern fringes. Proc SPIE 2006;6252.
[23] Ghiglia D, Pritt M. Two-dimensional phase unwrapping: theory, algorithms and software. New York: Wiley; 1998.
[24] Dias J, Leitao J. The ZπM algorithm for interferometric image reconstruction in SAR/SAS. IEEE 2001;20(5).